New Journal of Physics
An Institute of Physics and Deutsche Physikalische Gesellschaft Journal

On the detection of Reynolds stress as a driving and damping mechanism of geodesic acoustic modes and zonal flows

M Ramisch[1], U Stroth[1], S Niedner[1,2] and B Scott[2]

[1] IEAP, University of Kiel, 24098 Kiel, Germany
[2] MPI für Plasmaphysik, EURATOM Association, Garching, Germany
E-mail: stroth@physik.uni-kiel.de

New Journal of Physics **5** (2003) 12.1–12.11 (http://www.njp.org/)
Received 24 October 2002
Published 4 February 2003

Abstract. Bispectral analysis has been proposed as a diagnostic for Reynolds stress (RS) as a driving mechanism of zonal flows (ZF) in toroidally confined plasmas. A turbulence simulation code was used to test this technique on a well-defined system. It turned out that the geodesic acoustic mode dominates the poloidal flow spectrum and that it reduces radial transport in the same way as does a low-frequency ZF. Using the total cross-bicoherence, a correlation between RS and large-scale poloidal flows could be detected. The experimentally more accessible auto-bicoherences did not prove to be a useful quantity for studying this interaction. RS was not observed as a precursor of the flow; rather it appears simultaneously in the region of radial flow shear.

Contents

PII: S1367-2630(03)55215-6

1. Introduction

Zonal flows (ZF) are poloidally and toroidally symmetric ($k_\theta = k_\parallel = 0$), radially localized ($k_r \neq 0$) potential structures [1, 2]. They can be described as low-frequency $\tilde{\boldsymbol{E}} \times \boldsymbol{B}$ shear flows and therefore play an important role in turbulent transport. ZFs limit the radial correlation length via the shear decorrelation mechanism [3] and can trigger transitions into transport barriers. In this work it turns out that ZFs come in two types: low-frequency flows, which were originally considered for turbulence decorrelation, and flows at the geodesic acoustic mode (GAM) frequency, which should appear together with the pressure side-band $\tilde{p} = p_0 \sin(\theta)$. The term ZF is used for both types of flow. If a distinction is needed, the terms GAM and low-frequency ZF are used explicitly. The GAM is a result of poloidal pressure asymmetries, which are induced by poloidal $\boldsymbol{E} \times \boldsymbol{B}$ rotation. The dominant restoring force is due to the radial component of the diamagnetic current which appears because of the displacement of the pressure contours with respect to the flux surfaces. In wavenumber space, the structure of the ZF and the GAM is the same. The difference occurs in frequency space. It will turn out that the GAM is the dominant flow in this analysis.

It has been proposed that the drive of ZFs is due to Reynolds stress (RS) [4]. This has been considered as a mode-coupling problem in which the energy of small-scale radial and poloidal velocity fluctuations $\tilde{v}_r$, $\tilde{v}_\theta$ is transferred to the large-scale ZF V_θ via three-wave interactions [5]–[8]. Treated as a mode-coupling problem the ZF generation turns out to be related to the cross-bispectrum of these quantities [5], namely $\tilde{v}_r$, $\tilde{v}_\theta$ and the ZF potential Φ, defined as $B(\omega_1, \omega_2) = \langle \hat{v}_r(\omega_1)\hat{v}_\theta(\omega_2)\hat{\Phi}^*(\omega_1 + \omega_2)\rangle$. Experimental investigations of the driving mechanism of ZFs are difficult to carry out, since in order to obtain the quantities $\tilde{v}_r$, $\tilde{v}_\theta$, V_θ expensive multipoint measurements in time and in space are required. The limitation to the auto-bispectrum of potential and density fluctuations [6, 7] provides an experimentally more accessible quantity, since single point measurements are sufficient for temporal Fourier analysis. It must be noted, however, that $\tilde{n}$ and $\tilde{\phi}$ have different nonlinear properties [9].

Since the measurement of bicoherence is a very ambitious task, it is worthwhile testing this technique on a well-defined system like a turbulence simulation code. Simulations have the advantage that all the information is available. Hence simplified forms of the bicoherence can be checked against the full form. Furthermore, since the simulation is carried out on a spatial grid, equivalent grid points as in the poloidal direction can be used to perform sample averages. Hence the causality between RS and ZF can be studied much more carefully than in experiment, where the sample average has to be done in time.

The objective of this paper is twofold. First, the results from a turbulence simulation code are used to investigate the RS as a driving mechanism of ZFs. The analysis is done by different bispectral quantities which have been predicted to be related to the ZF generation. Second the applicability of these different bispectral quantities as a diagnostic of ZF drive is investigated.

In section 2 the simulation code is introduced. Section 3 describes the different bispectral analysis tools. In section 4 the simulation data are analysed for ZFs and in section 5 the relation to the bispectral quantities is investigated. The results are discussed in section 6.

2. The simulation code DALF3

The drift Alfvén turbulence code DALF3 [10] solves a two-fluid model in three-dimensional flux tube geometry. The model includes interchange and drift wave turbulence, which is coupled

to shear Alfvén waves. The dependent variables are fluctuations in electrostatic potential ($\tilde{\phi}$), electron density ($\tilde{n}_e$), parallel current ($\tilde{J}_\parallel$) and parallel ion flow ($\tilde{u}_\parallel$), with the parallel magnetic potential ($\tilde{A}_\parallel$) given through Ampère's law. The equations read

$$\frac{n_e M_i c^2}{B^2}\frac{\mathrm{d}}{\mathrm{d}t}\nabla_\perp^2\tilde{\phi} = \nabla_\parallel \tilde{J}_\parallel - \mathcal{K}(\tilde{p}_e), \tag{1}$$

$$\frac{n_e e}{c}\frac{\partial}{\partial t}\tilde{A}_\parallel + \frac{m_e}{e}\frac{\mathrm{d}}{\mathrm{d}t}\tilde{J}_\parallel = \nabla_\parallel(p_e + \tilde{p}_e) - n_e e\nabla_\parallel\tilde{\phi} - 0.51\frac{m_e}{e}\nu_e\tilde{J}_\parallel, \tag{2}$$

$$\frac{\mathrm{d}}{\mathrm{d}t}(\tilde{p}_e + p_e) = \frac{T_e}{e}\nabla_\parallel\tilde{J}_\parallel - p_e\nabla_\parallel\tilde{u}_\parallel - \frac{T_e}{e}\mathcal{K}(\tilde{p}_e) + p_e\mathcal{K}(\tilde{\phi}), \tag{3}$$

$$n_i M_i\frac{\mathrm{d}}{\mathrm{d}t}\tilde{u}_\parallel = -\nabla_\parallel(p_e + \tilde{p}_e). \tag{4}$$

This set consists of equations for the conservation of charge (1), parallel electron (2) and ion momentum (4) and energy (3), where

$$\frac{\mathrm{d}}{\mathrm{d}t} = \frac{\partial}{\partial t} + \frac{c}{B^2}\boldsymbol{B}\times\nabla\phi\cdot\nabla, \qquad \mathcal{K} \equiv -\nabla\cdot\frac{c}{B^2}\boldsymbol{B}\times\nabla. \tag{5}$$

m_e, p_e and e are the electron mass, the electron pressure and the electron charge, and ν_e is the Braginskii electron collision frequency [11]. T_e is the background electron temperature and M_i is the ion mass. Electric and magnetic field fluctuations are coupled by the Maxwell equations.

The equations are solved in a flux tube modelling closed flux surface tokamak geometry, with globally consistent boundary conditions [12] and using a 'shifted metric' technique to represent both slab and toroidal eigenmode types equally well [13]. The background density and magnetic pitch parameter (q) are both given gradients ($L_\perp = |\nabla\log n_e|^{-1}$, hence $p_e = -x/L_\perp$ under $\mathrm{d}/\mathrm{d}t$ and $\nabla_\parallel$, and $\hat{s} = rq'/q$, respectively); the equations are otherwise homogeneous. The coordinates x and y describe the drift plane perpendicular to the magnetic field $\boldsymbol{B}$, similar to but importantly different from the poloidal (r,θ) plane. The coordinate z projects the position along $\boldsymbol{B}$ onto the poloidal location θ, so that the flux tube samples the entire poloidal structure (hence, the perpendicular angle coordinate, y, actually tracks the toroidal position although its gradient is nearly poloidal; see [12] for details).

The turbulence resulting from the equations is controlled by the dimensionless parameters

$$\hat{\mu} = \frac{m_e}{M_i}\left(\frac{qR}{L_\perp}\right)^2 \qquad \hat{\beta} = \frac{4\pi n_e T_e}{B^2}\left(\frac{qR}{L_\perp}\right)^2 \qquad \hat{\nu} = 0.51\nu_e\frac{L_\perp}{c_s} \tag{6}$$

where R is the toroidal major radius and c_s is the sound speed given by $c_s^2 = T_e/M_i$. The significance of the three parameters is, respectively, the ability of the turbulence to compete with the long ($\hat{\beta}$) and short ($\hat{\mu}$) wavelength limits of the Alfvén response, and the relative collisionality. All three parameters are typically greater than unity for edge turbulence.

From the potential fluctuations the contravariant components of the $\boldsymbol{E}\times\boldsymbol{B}$ velocity are found according to $\tilde{v}^x = -(\partial\tilde{\phi}/\partial y)$ and $\tilde{v}^y = (\partial\tilde{\phi}/\partial x)$. The mean flow has only a y-component, found from the flux surface averaged (over y and z) potential $\Phi = \langle\phi\rangle_{y,z}$ according to $V^y = (\partial\Phi/\partial x)$. The flux surface averaged turbulent transport is $\Gamma^x = \langle\tilde{n}_e\tilde{v}^x\rangle$.

In this paper the results are presented in physical units with respect to $L_\perp = 5$ cm and geometrical parameters of the Kiel torsatron TJ-K as presented in [14, 15], offering the possibility of direct comparison with experimental results in future work.

3. Zonal flows and bispectral analysis

Details of bispectral analysis of experimental data have been given elsewhere [16]. The method is briefly summarized here. The normalized cross-bicoherence of three fluctuating parameters f, g, h is given by

$$b^2_{fgh}(\omega_1, \omega_2) = \frac{|B_{fgh}(\omega_1, \omega_2)|^2}{\langle|\hat{f}(\omega_1)\hat{g}(\omega_2)|^2\rangle\langle|\hat{h}(\omega_3)|^2\rangle}, \tag{7}$$

where

$$B_{fgh}(\omega_1, \omega_2) = \langle\hat{f}(\omega_1)\hat{g}(\omega_2)\hat{h}^*(\omega_3)\rangle \tag{8}$$

is the cross-bispectrum, evaluated at the resonance condition $\omega_3 = \omega_1 + \omega_2$, $\hat{f}$ is the Fourier transform of f, '*' denotes the complex conjugate and $\langle\cdot\rangle$ averaging over a large number of realizations of the spectral function inside the brackets. In particular, the auto-bicoherence and the auto-bispectrum of a single parameter f is obtained by replacing g and h in (7) and (8) by f.

The bispectrum measures the degree of phase coherence between three modes at ω_1, ω_2 and ω_3 (i.e. the degree of a fixed phase relation between these modes). The bicoherence gives the respective normalized measure. A measure of the relative contribution of a mode at ω_3 in coherent three-mode coupling is provided by the integrated bicoherence

$$b^2(\omega_3) = \sum_{\omega_1,\omega_2} b^2(\omega_1, \omega_2)\,\delta_{\omega_1+\omega_2,\omega_3}. \tag{9}$$

For the purpose of temporal or spatial comparisons the total integrated bicoherence

$$b^2 = \sum_{\omega_3} b^2(\omega_3) \tag{10}$$

provides a measure of the total amount of coherent three-mode coupling.

From fluid theory it follows that the energetic drive term for ZFs is given by $\langle\Omega\rangle_{y,z}\langle\tilde{v}^x\tilde{v}^y\rangle_{y,z}$ [17, 18], where $\langle\cdot\rangle_{y,z}$ stands for the zonal average. The quantity relates the RS to the vorticity Ω and can be represented as the cross-bispectrum $B_{v^x v^y \Phi}(\omega_1, \omega_2)$ [5] under the resonance condition for the frequencies, where $\omega_3 = \omega_{\mathrm{ZF}} \approx 0$. In order to study the energy transfer between modes, $\langle\Omega\rangle_{y,z}\langle\tilde{v}^x\tilde{v}^y\rangle_{y,z}$ has to be decomposed in wavenumber space. Hence, the physical process happens in k not in ω space. In this case, the resonance condition applies to the wavevectors $\boldsymbol{k}_3 = \boldsymbol{k}_1 + \boldsymbol{k}_2$, where $\boldsymbol{k}_3 = \boldsymbol{k}_{\mathrm{ZF}}$ with $k_{\mathrm{ZF},\theta} = k_{\mathrm{ZF},\parallel} = 0$. The correlation between the ZF, vorticity and the RS should be reflected in the respective total integrated bicoherences. The summation in (10) has to be restricted to the low frequencies of the ZF. In wavenumber space we restrict ourselves to the poloidal wavenumber $k_3 = k_{\mathrm{ZF},\theta} = 0$.

For the experimental study of ZF generation as a mode-coupling problem, alternative bispectral quantities—the auto-bispectrum of potential and density fluctuations in frequency space—have been derived in [6, 7]. Accordingly the generation of ZFs is also supposed to be reflected in an increase in the respective total integrated auto-bicoherence, which would provide an experimentally more accessible quantity.

In tokamak devices an increase in the amount of three-wave coupling has been observed during L–H transitions as a precursor of $\boldsymbol{E} \times \boldsymbol{B}$ shear flow development [6, 7]. A similar type of correlation between three-wave coupling and ZF-like structures has been reported in [19]. In this case the non-ambipolarity of the turbulent transport was important for generating the ZF. So far no clear proof exists that three-wave coupling is responsible for ZF generation.

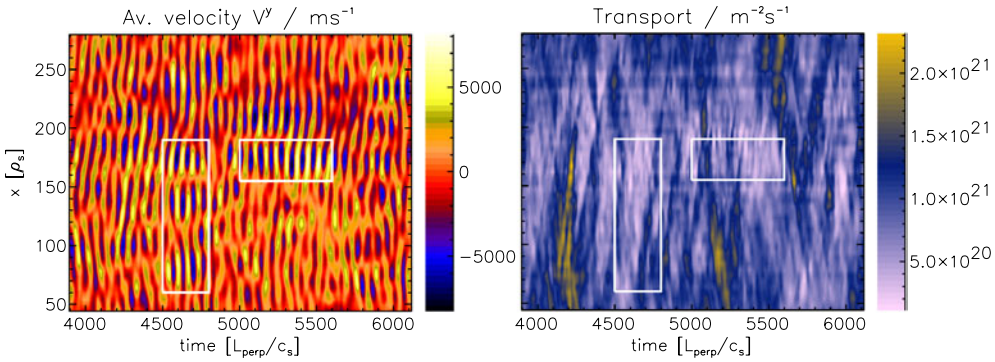

Figure 1. (t, x)-profiles of average poloidal flow (left) and radial transport (right) calculated from a simulation run with parameters $\hat{\beta} = 0.7$, $\hat{\nu} = 4.0$. The dominant flow oscillations are due to GAMs. Regions with the highest values of V^y are marked by boxes. They are characterized by the highest contrast. Transport minima are found in the vicinity of these flow maxima.

4. Analysis of zonal flows

In a first step, the simulated data for various values of $\hat{\beta}$ and $\hat{\nu}$ were analysed to detect ZFs. Turbulence properties of these data have been analysed in [14]. In this paper results of simulation runs are analysed whose control parameters basically belong to the drift wave regime. The other parameters are $\hat{\mu} = 1.1$ and $\epsilon_s = (qR/L_\perp)^2 = 2025$. With $L_\perp = 5$ cm this refers to hydrogen gas.

Figure 1 shows contour profiles of the average poloidal flow V^y and the radial transport Γ^x calculated from a simulation run with $\hat{\beta} = 0.7$ and $\hat{\nu} = 4.0$. For the calculation of the average in the z direction only two planes were used: one at the magnetic low-field side and one at the high-field side.

The most apparent feature is a periodic oscillation in the entire radial range. To examine these oscillations, an arbitrary segment of a time trace at a fixed position x is shown in figure 2 (left). It turns out that the characteristic frequency of the oscillation is approximately consistent with $f \approx 0.015\, c_s/L_\perp$. It appears as a peak in the frequency spectrum of V^y shown in figure 2 (right). The spectrum was obtained by averaging the spectra of all time traces in figure 1 (left). The frequency agrees rather well with the prediction for GAMs [20], which is given by $\omega_{\mathrm{GAM}} = \sqrt{2}\, c_s/R = \omega_B\, c_s/(\sqrt{2}\, L_\perp)$, where $\omega_B = 2L_\perp/R$. For the parameters used this yields $f_{\mathrm{GAM}} = 0.0146\, c_s/L_\perp$. The low-frequency ZF appears as a smaller peak in the averaged spectrum. Further simulation runs with $\hat{\nu} = 1.0$–6.0 holding $\hat{\beta} = 0.7$ fixed and with $\hat{\beta} = 0.7$–2.25 holding $\hat{\nu} = 4.0$ fixed have been analysed as well. In all cases a peak of the mean poloidal flow at the GAM frequency of $f \approx 0.015\, c_s/L_\perp$ was present. As expected for GAMs the frequency scales with c_s/R and not with $\hat{\beta}$ or $\hat{\nu}$. The relative amplitude of the low-frequency ZF and the GAM changes with time and location. But in all cases the GAM peak is at least of similar magnitude as the low-frequency peak. For comparison, another spectrum at a fixed position x is also shown on the right-hand side of figure 2.

The search for ZFs has revealed that GAMs, which can be considered as the damping mechanism of the ZFs [18], make the dominant contribution to the average poloidal flow. The GAMs are rather dominant fluctuations in the entire plasma and the ZFs rather show up as the

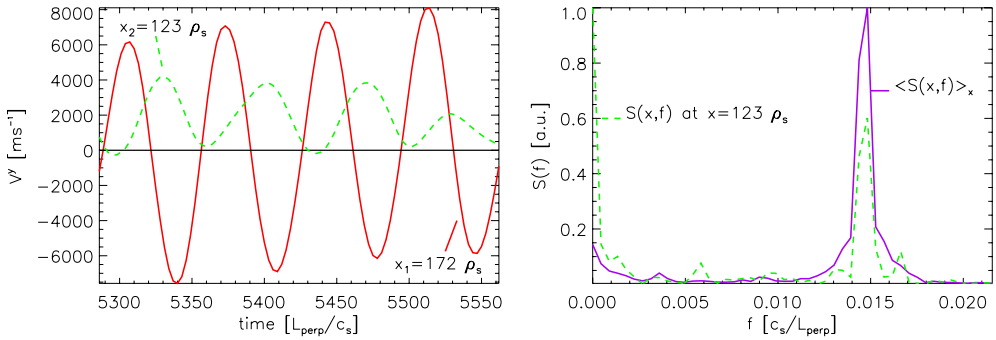

Figure 2. Segment of a time trace of V^y from figure 1 at fixed positions $x_{1,2}$ (left). The full curve belongs to a region with high values of V^y (x_1) and the dashed curve to a region with lower values (x_2). The oscillation has a period of $T \approx 70\, L_\perp/c_s$ reflected in the autopower spectrum of V^y (right) by a peak at $f \approx 0.015\, c_s/L_\perp$. Also a smaller peak at zero frequency is visible. For comparison another spectrum at fixed x is shown.

envelope of the GAM amplitude. However, the effect of GAMs on radial transport is similar to that of ZFs. This can be seen on the right-hand side of figure 1, where transport events with long radial correlation length are decorrelated when the GAM amplitude is large enough.

In order to examine the correlation of the radial transport with poloidal flow shear more quantitatively, a cross-correlation analysis was carried out. The degree of correlation as a function of the spatial lag Δx was calculated according to

$$\langle C_{uv}\rangle_t = \frac{1}{\tau}\int\!\!\int \frac{(u(x,t)-\langle u(x,t)\rangle_x)}{\sigma_{u,x}}\frac{(v(x+\Delta x,t)-\langle v(x,t)\rangle_x)}{\sigma_{v,x}}\,\mathrm{d}x\,\mathrm{d}t \qquad (11)$$

where σ denotes the respective standard deviation and τ the time window used for averaging. Interchanging x and t in (11) yields the degree of correlation as a function of the time lag Δt. Figure 3 shows the result for the temporally averaged (left) and the spatially averaged (right) cross-correlation between radial transport ($v = \Gamma^x$) and poloidal flow shear ($u = |\partial_x V^y|$). A clear anti-correlation is found in space and time. Regions with strong flow shear are related with regions of reduced radial transport. Furthermore, the reduction in transport is delayed by about $15\, L_\perp/c_s$ with respect to the maximum in flow shear. This points to the fact that the flow shear suppresses transport. Hence, the GAM has a similar effect on transport as the low-frequency ZF.

5. Relation of zonal flows with Reynolds stress

Reynolds stress (RS) as a possible driving mechanism of ZFs and GAMs has been investigated by means of cross-bicoherence analyses. The energetic drive of the ZF is given by the zonally averaged vorticity $\langle\Omega\rangle_{y,z}$ times the zonally averaged RS $\langle\tilde{v}^x\tilde{v}^y\rangle_{y,z}$ [17, 18]. As a measure of the correlation of small-scale turbulence with large-scale ZF/GAM the cross-bicoherence of fluctuations of velocity components $\tilde{v}^x$, $\tilde{v}^y$ and the temporally varying flow potential Φ can be used [1]. Here we use the flow shear instead of the flow potential, since the flow shear is exactly the zonally averaged vorticity.

All the information needed to calculate this expression is only available from simulated data. In experiments, a reduced number of data, sometimes even single point measurements,

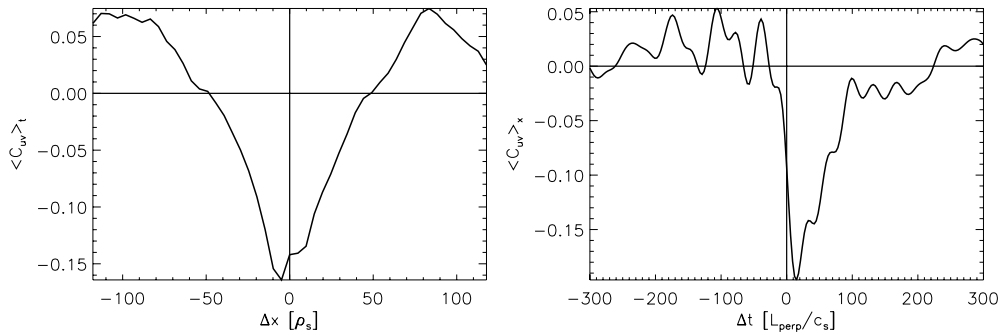

Figure 3. Temporally averaged cross-correlation $\langle C_{u,v}\rangle_t$ (left) and spatially averaged cross-correlation $\langle C_{u,v}\rangle_x$ (right) of radial transport $v = \Gamma^x$ with absolute flow shear $u = |\partial_x V^y|$. The anti-correlation between the flow shear and the radial transport is apparent.

have to be used. The objectives are to investigate whether there is a correlation if use can be made of the full data and if so whether the correlations also show up in a reduced data set as used, for example for the auto-bicoherence. Hence four different bicoherences are calculated: the full one using the appropriate velocities in k-($b_{v,k}$) and in frequency space ($b_{v,f}$) as well as auto-bicoherences in density (b_n) and potential (b_ϕ), which are both, of course, calculated in frequency space. In figures 4 and 5 the estimates for the total integrated bicoherences are compared with the poloidal flow and the flow shear.

Details of the data analyses are as follows: for the cross-bicoherence in wavenumber space the quantities $\tilde{v}^x$, $\tilde{v}^y$ and $\langle\Omega\rangle_{y,z}$ are calculated on a grid of 128 points in the y direction. Note that $\langle\Omega\rangle_{y,z}$ represents the value of the Fourier spectrum at $k_y = 0$. For averaging, 24 realizations are taken from a time window of size $T = 70\,L_\perp/c_s$. This corresponds to one GAM period. The resulting total integrated bicoherence $b_{v,k}$ is assigned to a point in time at the centre of the window, from which the realizations are taken.

Similarly the cross-bicoherence in frequency space is calculated: frequency spectra are calculated on time windows of size $T = 70\,L_\perp/c_s$ and 128 samples are averaged along the y coordinate, i.e. from 128 realizations the total integrated bicoherence $b_{v,f}$ is calculated and assigned to one point in time determined by the centre of the time window. The integrated bicoherence is calculated in a small range around $\omega = 0$. A sliding window is used for temporal resolution.

Using the same method, the total integrated auto-bicoherences of potential and density fluctuations b_ϕ and b_n are calculated: time windows with a length $T = 70\,L_\perp/c_s$ are applied to time series and averaging is done along the y direction resulting in an average over 128 realizations.

The results shown in figures 4 and 5 are from the area indicated by the horizontal box in figure 1. The profiles of the total integrated cross- and auto-bicoherences are shown in the top row. The magnitudes are depicted in units of the respective noise level. In the middle the profiles of the average poloidal flow are overlaid with contour lines of the bicoherence profiles from the top. The bottom row shows the overlay of the flow shear profiles with these contour lines. Figure 4 refers to the cross-bicoherences $b_{v,f}$ (left column) and $b_{v,k}$ (right column) and figure 5 refers to the auto-bicoherences b_ϕ (left column) and b_n (right column).

The overlay of the flow and the vorticity (flow shear) profiles with contours of $b_{v,f}$ in figure 4

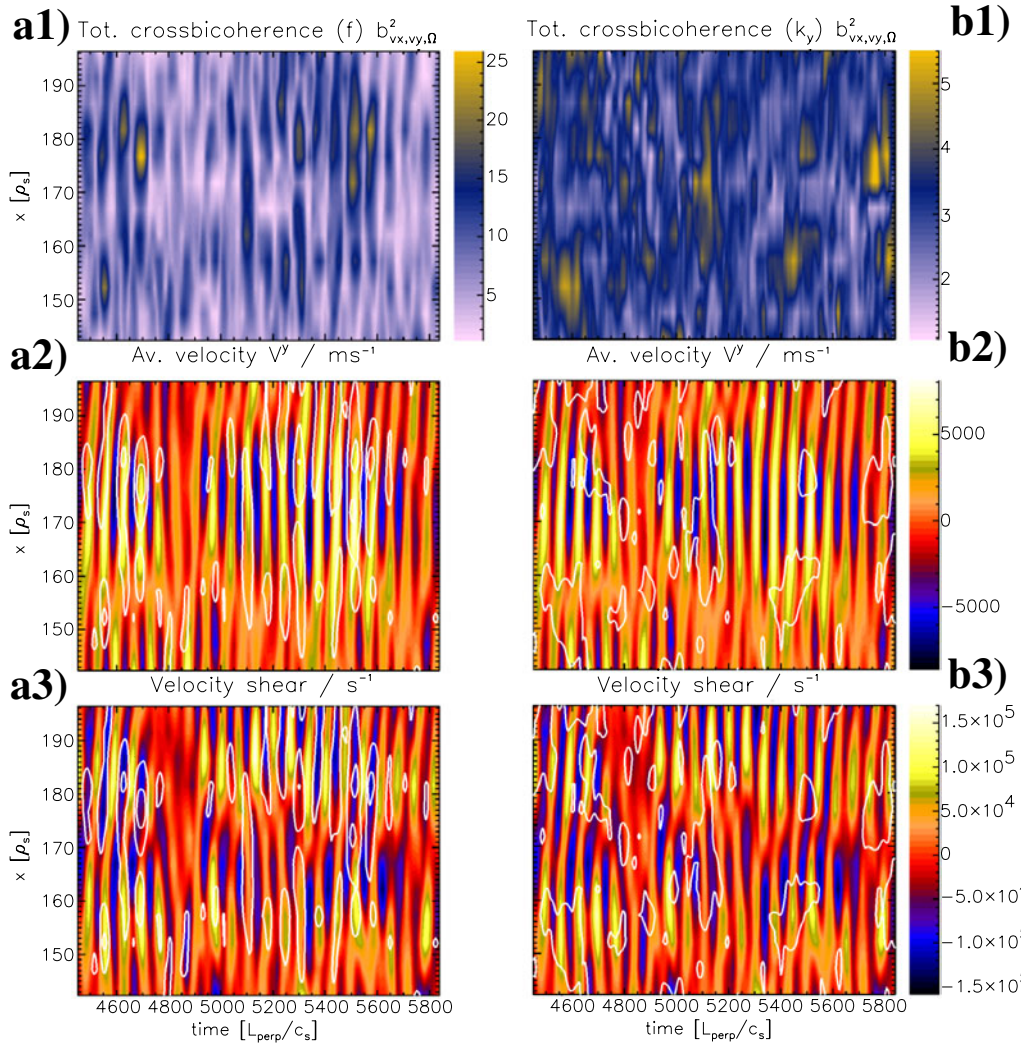

Figure 4. (t, x) profiles of total integrated cross-bicoherences in comparison with the average poloidal flow and the flow shear. The left column refers to $b_{v,f}$ (a1) and the right column to $b_{v,k}$ (b1). Contours from both quantities are overlaid on the flow V^y (a2, b2) and the flow shear $\partial_x V^y$ (a3, b3) profile. High values of $b_{v,f}$ are located at high values of the flow shear.

clearly shows that high values of this bispectral quantity exist in the vicinity of high flow values and coincide in rather good agreement with high values of the flow shear. $b_{v,f}$ is in phase with the flow shear on the high-pressure side (small x) and out of phase on the low-pressure side. This is due to the fact that the bicoherence is positive by definition while the flow shear changes its sign. In wavenumber space the correlation of $b_{v,k}$ with the flow or the flow shear is not as clear as in frequency space.

The auto-bicoherence b_ϕ in figure 5 (left) does not show any correlation with the flow or the flow shear. The bicoherence b_n related to density fluctuations (figure 5, right), on the other hand, has regions with a large number of three-mode interactions, which irregularly overlap with regions of high flow shear. This might be related to the fact that the GAM appears as a pressure

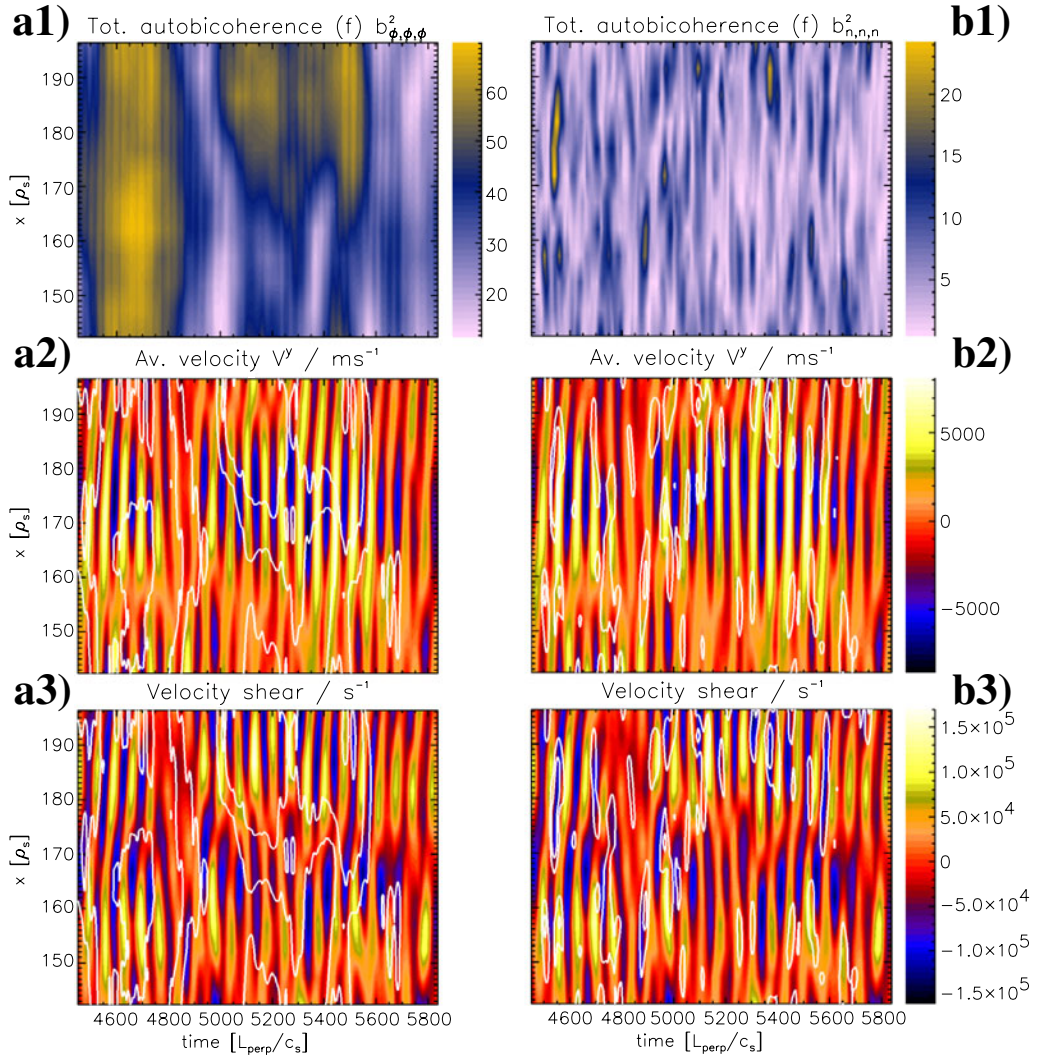

Figure 5. (t, x) profiles of total integrated auto-bicoherences in comparison with the average poloidal flow and the flow shear in the same representation as in figure 4. The left column refers to b_ϕ (a1) and the right column to the b_n (b1), both calculated in frequency space. A correlation with the flow or the flow shear is not observable in the case of b_ϕ. The bicoherence related to density fluctuations reveals an irregular conformance with the flow shear.

perturbation in the poloidal direction.

For a quantitative analysis, cross-correlations between the bicoherences and the absolute amplitude of the flow shear were calculated according to equation (11), where x and t have to be interchanged. The results for the spatially averaged cross-correlation $\langle C_{u,v}\rangle_x$ are shown in figure 6. The qualitative results from figures 4 and 5 are confirmed. The only quantity with a reasonable correlation of 25% is the full bicoherence calculated in frequency space. A time lag, which would be an indication of RS drive of the flows, is not observed. However, the width of the correlation function is larger than the GAM period and is asymmetric. This might point to some correlation of RS drive with the zero-frequency component of the ZF, which always has

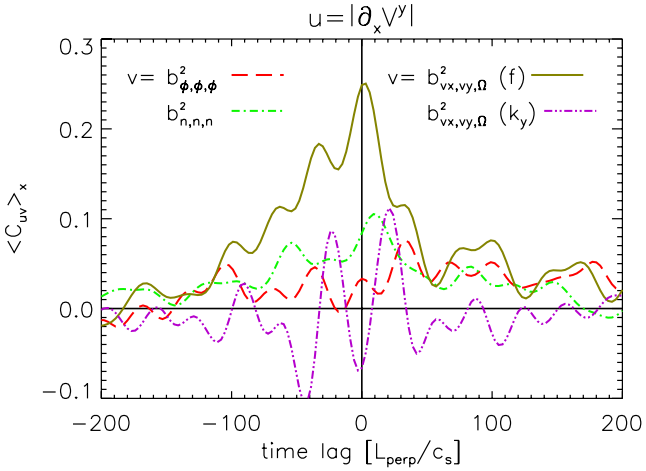

Figure 6. Spatially averaged cross-correlations $\langle C_{u,v}\rangle_x$ of respective bicoherences with absolute flow shear $u = |\partial_x V^y|$. A reasonable correlation of 25% is found between the flow shear and the cross-bicoherence $b_{v,f}$ at $\Delta t = 0$.

some amplitude in the system. The correlation of the flow shear with the bicoherence calculated in k space is less than 15%. The cross-correlations between the bicoherences and the flow itself are below 10%.

6. Summary and conclusions

Data obtained from the drift Alfvén turbulence simulation code DALF3 were analysed for ZF. The autopower spectrum of the flux-surface averaged poloidal flow shows two major contributions, a peak at zero frequency and a second peak at the frequency of the GAM, which scales with c_s/R. The mean poloidal flow is clearly dominated by the GAM oscillations. Hence, the ZFs come in two types, a low-frequency ZF ($\omega = 0, k_y = 0$), which was originally considered for turbulence decorrelation, and flows at the GAM frequency ($\omega \neq 0, k_y = 0$). The GAMs can be considered as a damping mechanism of the low-frequency ZFs. It was demonstrated that the flow shear due to the GAMs also contributes to a reduction in radial transport. The maximum in flow shear was found to occur prior to a reduction in transport.

In the simulation, the drive of ZFs is due to RS. The drive of the GAM by RS should actually be stronger than that of the low-frequency ZF. Bispectral methods have been suggested as an appropriate tool for experimental study of this mechanism. The total integrated cross-bicoherence of $\boldsymbol{E} \times \boldsymbol{B}$ velocity fluctuations $\tilde{v}^x$, $\tilde{v}^y$ and the zonally averaged vorticity $\langle\Omega\rangle_{y,z}$ is a measure of the correlation between the mean poloidal flow and the RS. In order to investigate the efficiency of this technique, different bispectral analyses were carried out on the simulated data.

The strongest correlation was found when the analysis was carried out in frequency space. The spatial and temporal evolution of flow shear coincides with an increased number of three-mode interactions indicated by the total integrated cross-bicoherence. The cross-correlation between the bicoherence and the flow shear is about 25% when averaged over the radial coordinate. The correlation function is broader than the GAM period and is asymmetric. This could be a hint to RS drive of the low-frequency ZF. The analysis in k space did not show any clear relation between flow and bicoherence.

In experimental investigations, the use of the auto-bispectrum would be much more appropriate. However, no clear correlation of the mean poloidal flow and the total integrated auto-bicoherence of plasma potential or density fluctuations was found. In the case of the auto-bicoherence of density fluctuations some relation with the flow shear was found, which might be related to the pressure perturbation of the GAM.

In summary, the GAM was found to be the dominant poloidal flow in the simulation data with a similar effect on radial transport as the low-frequency ZF. A correlation between RS and ZF/GAM could only be detected in the cross-bicoherence taken in frequency space. The auto-bicoherences do not appear as a useful quantity to study the interaction of RS and ZF/GAM. RS has not been observed as a clear precursor of strong ZF or GAM amplitudes. It rather appears simultaneously in the region of radial ZF and GAM gradients. Although the RS is the only mechanism in the code driving large-scale ZFs, in the bispectral analysis the RS could not be detected as such.

Acknowledgment

This work is financially supported by the Max-Planck Institut für Plasmaphysik, EURATOM Association.

References

[1] Diamond P H *et al* 1998 Fusion energy *Proc. 17th Int. Conf. (Yokohama, Japan, 1998)* (IAEA: Vienna) No TH3/1
[2] Terry P W 2000 *Rev. Mod. Phys.* **72** 109
[3] Hahm T S *et al* 1999 *Phys. Plasmas* **6** 922
[4] Diamond P H and Kim Y B 1991 *Phys. Fluids* B **3** 1626
[5] Diamond P H *et al* 2000 *Phys. Rev. Lett.* **84** 4842
[6] Moyer R A, Tynan G R, Holland C and Burin M J 2001 *Phys. Rev. Lett.* **87** 135001(4)
[7] Tynan G R, Moyer R A, Burin M J and Holland C 2001 *Phys. Plasmas* **8** 2691
[8] Scott B 2000 *Theory of Fusion Plasmas* ed J Connor, O Sauter and E Sindoni (Bologna: Editrice Compositori) p 413
[9] Hasegawa A and Wakatani M 1983 *Phys. Rev. Lett.* **50** 682
[10] Scott B 1997 *Plasma Phys. Control. Fusion* **39** 1635
[11] Braginskii S I 1965 *Reviews of Plasma Physics* ed M A Leontovich (New York: Consultants Bureau) p 205
[12] Scott B 1998 *Phys. Plasmas* **5** 2334
[13] Scott B 2001 *Phys. Plasmas* **8** 447
[14] Niedner S, Scott B D and Stroth U 2002 *Plasma Phys. Control. Fusion* **44** 397
[15] Lechte C, Niedner S and Stroth U 2002 *New J. Phys.* **4** 34.1
[16] Kim Y C and Powers E J 1979 *Trans. Plasma Sci.* **7** 120
[17] Hallatschek K and Biskamp D 2001 *Phys. Rev. Lett.* **86** 1223
[18] Scott B 2003 *Phys. Lett.* A submitted
(Scott B 2002 *Preprint* physics.plasm-ph/0208026)
[19] Shats M G and Solomon W M 2002 *Phys. Rev. Lett.* **88** 045001(4)
[20] Winsor N, Johnson J L and Dawson J M 1968 *Phys. Fluids* **11** 2448